www.czasopisma.pan.pl PAN www.journals.pan.pl

ARCHIVES of FOUNDRY ENGINEERING

ISSN (2299-2944)
Volume 19
Issue 3/2019

33 – 37

10.24425/afe.2019.127135

6/3

Published quarterly as the organ of the Foundry Commission of the Polish Academy of Sciences

Research on the Characterization of Ti Inclusions and Their Precipitation Behavior in Tire Cord Steel

Jialiu Lei *, Dongnan Zhao, Yongjun Fu, Xianfeng Xu
Hubei Polytechnic University
16 Guilin N Rd, Xialu Qu, Huangshi Shi, Hubei Sheng, Chiny
* Corresponding author. E-mail address: 710158466@qq.com

Received 14.05.2019; accepted in revised form 03.06.2019

Abstract

In the present investigation, the morphology of Ti inclusions in high strength tire cord steel was investigated and their precipitation behavior was discussed using a precipitation and growth model. The results show that Ti inclusions mainly exist in the form of TiN. The two-dimensional characterization of Ti inclusions is square-like with sharp edges and corners, while its three-dimensional shape exhibits a cubic or rectangular-prism morphology. The Ti inclusions do not precipitate when the solid fraction of tire cord during solidification is less than 0.987, and their final radius is closely related to the cooling rate and initial concentration product. The higher the cooling speed, the smaller the final radius, when the cooling speed is constant, the final radius of Ti inclusions is mainly determined by the initial concentration product, $w[N]_0 \times w[Ti]_0$. In order to retard the precipitation and growth of Ti inclusions in tire cord steel, the cooling rate and initial concentration product can be taken into consideration.

Keywords: Characterization, Precipitation behavior, Ti inclusions, Concentration product, Tire cord steel

1. Introduction

As a superior quality product of wire rod, tire cord steel is mainly used in radial ply tyres. Its outstanding mechanical performances, such as its excellent elasticity, high strength, long service life, and impact resistance, are necessary [1,2]. It is a pivotal mission to improve the steel purity in the production.

Before tire cord is made, the steel wire is drawn from 5.5 mm to 0.15 mm in diameter and subjected to cyclic stress in the drawing and twisting process. Therefore, the breakage of steel wire during fabrication is a crucial issue. It has been shown that if the size of non-metallic inclusions in steel cord is greater than 2% of the diameter of the processing wire, it causes breakage of the steel wire. This filament break is especially sensitive with the existence of angular and non-deformable Ti inclusions, such as TiN or Ti(CN), which act as cleavage initiators [3,4]. This causes fracture delamination in the drawing and twisting process for steel wire or decreases the fatigue performance and seriously affects traffic safety [5]. It has been one of the main challenges in tire cord steel production, especially for high-strength or ultra-high-strength tire cord steel [6,7]. Therefore, internationally recognized companies, such as Bekaert, proposed the penalty point specification of Ti inclusions to judge wire rods [8]. With the improvement of strength grade for tire cord steel, the effective control of Ti inclusions has become more and more crucial.

In this study, grade-80 tire cord steel is researched by an industrial experiment combined with the formation thermodynamics and dynamics. Then the characterization of Ti inclusions and their precipitation behavior are further revealed.

2. Experimental Aspects

The chemical composition of grade-80 tire cord steel slab is 0.82 wt% C, 0.19 wt% Si, 0.5 wt% Mn, 0.009 wt% P, 0.009 wt% S, 0.0011 wt% Als, 0.0017 wt% O, 0.0039 wt% N, 0.0008 wt% Ti and balance Fe, respectively. In order to gain a greater understanding of Ti inclusions, rectangular pieces (20 mm×20 mm×20 mm thickness) and cylindrical samples 10 mm in diameter and 120 mm high were cut from the billet, which was not rolled. The former were employed for two-dimensional (2D) observation and the latter for three-dimensional (3D) observation. After polishing, the characterization of Ti inclusions was observed by scanning electron microscopy (SEM) equipped with energy dispersive (EDS).

In order to clearly observe the 3D morphology of Ti inclusions, the polished cylindrical samples (φ10×120 mm) were placed in the device as shown in Figure 1, for the non-aqueous solution electrolysis experiment after cleaning.

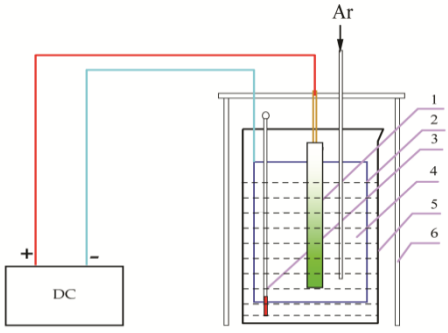

Fig. 1. Schematic diagram of non-aqueous solution electrolysis (1 sample, 2 cathode, 3 thermometer, 4 electrolyte, 5 electrolytic cell, 6 stents)

The electrolytic temperature was 273-278 K and current density was 50 mA/cm^2. In the experimental process, Argon was used to stir the electrolyte. After 4 hours of electrolysis, the inclusions from the electrolytic sample were separated via ultrasonic cleaning. With this method, the 3D morphology of Ti inclusions can be obtained.

3. Results and Discussion

3.1 Characterization of Ti Inclusions

The typical morphology of Ti inclusions in tire cord steel is shown in Figure 2. The 2D characterization of Ti inclusions shows that they have a square shape with sharp edges and corners and the 3D shape of Ti inclusions extracted by the non-aqueous solution electrolytic method exhibits a cubic or rectangular-prism morphology. The Ti inclusions are of a block type with a size less than 5 μm. The mapping analysis results indicated that the Ti inclusion mainly consisted of N and Ti elements.

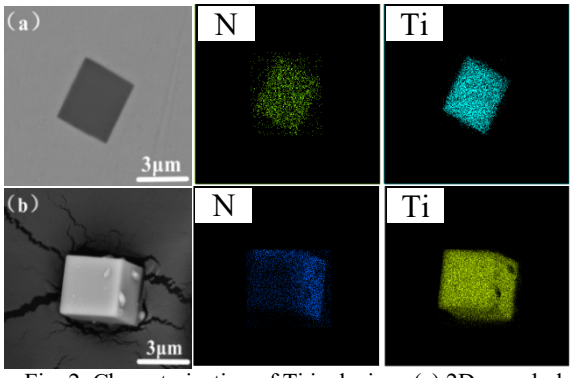

Fig. 2. Characterization of Ti inclusions (a) 2D morphology of Ti inclusions, (b) 3D morphology of Ti inclusions

3.2 Thermodynamic Calculations of Ti Inclusion Precipitation Behaviour

To provide a better clarity of the precipitation behavior of Ti inclusions, thermodynamic calculations for tire cord steel have been performed. The above characterization studies indicate that Ti inclusions mainly exist in the form of TiN, and this was taken into account for the calculations.

According to the chemical composition of the steel, the solidus and liquidus temperatures (K) can be obtained by Equations (1) and (2) [9], where $w[i]$ is the mass percentage of solute element i (wt%) .

$$T_L=1809\text{-}65w[C]\text{-}8w[Si]\text{-}5w[Mn]\text{-}30w[P]\text{-}25w[S]\text{-}3w[Al]\text{-}20w[Ti]\text{-}90w[N]\text{-}80w[O] \quad (1)$$

$$T_S=1809\text{-}175w[C]\text{-}20w[Si]\text{-}30x[Mn]\text{-}280w[P]\text{-}575w[S]\text{-}7{,}5w[Al]\text{-}40w[Ti]\text{-}160w[O] \quad (2)$$

Thermodynamic calculation of the precipitation of TiN inclusions in tire cord steel is given as follows [10]:

$$[\mathrm{Ti}]+[\mathrm{N}]=\mathrm{TiN}_{(s)}\ \ \Delta G^0=-291000+107.91T(\mathrm{J/mol}) \quad (3)$$

During the precipitation of TiN inclusions, the actual change of Gibbs free energy can be calculated by the following formula:

$$\Delta G=\Delta G^0+RT\ln\frac{a_{\mathrm{TiN}}}{a_{\mathrm{N}}a_{\mathrm{Ti}}}=\Delta G^0+RT\ln\frac{1}{f_{\mathrm{N}}w[\mathrm{N}]f_{\mathrm{Ti}}w[\mathrm{Ti}]} \quad (4)$$

Where a_{TiN}, a_{N}, and a_{Ti} denote the activities of TiN, N, and Ti, respectively. For pure TiN inclusions, $a_{\mathrm{TiN}}=1$. R is the ideal gas constant, whose value is 8.314 J/(mol·K). The activity coefficients f_{N} and f_{Ti} in liquid steel can be calculated by Equation (5) and the interaction coefficients e_i^j are given in Table 1 [11, 12].

$$\lg f_{\mathrm{i}}(1873\mathrm{K})=\sum e_i^j w[j] \quad (5)$$

Table 1.
Interaction coefficients in liquid steel at 1873 K

e_i^j	C	Si	Mn	P	S	Al	O	N	Ti
N	0.13	0.047	-0.021	0.045	0.007	-0.028	0.05	0	-0.537
Ti	-0.165	0.056	0.0043	-0.064	-0.11	0.12	-1.8	-1.8	0.013

The effect of temperature on activity coefficients is given by the following equations [9,13,14]:

$$\lg f_{\mathrm{N}}(T) = (\frac{3280}{T} - 0.75)\lg f_{\mathrm{N}}(1873\mathrm{K}) \tag{6}$$

$$\lg f_{\mathrm{Ti}}(T) = (\frac{2557}{T} - 0.365)\lg f_{\mathrm{Ti}}(1873\mathrm{K}) \tag{7}$$

As solidification continues, the redistribution of solute atoms results in microsegregation because of the different diffusion rates between liquid and solid phases. The segregation of N and Ti in micro-regions can be expressed by the following formulas [15]:

$$C_L = C_0(1 - (1 - \frac{\beta k}{1+\beta})g)^{(k-1)/(1-\beta k/(1+\beta))} \tag{8}$$

$$\beta = \frac{4D_S\tau}{L^2} \tag{9}$$

Where C_L is the actual mass concentration (wt%); C_0 denotes the initial chemical composition; k represents the balanced distribution coefficient between solid and liquid phases; g denotes the solid fraction; D_S is the diffusion rate in solid phase (cm^2/s); L represents the secondary dendrite spacing (μm); and τ represents the local solidification time (min). The solid-liquid interface temperature, T_{L-S} (K), can be calculated by Equation (10) [16]:

$$T_{L-S} = T_M - \frac{T_M - T_L}{1 - g\frac{T_L - T_S}{T_M - T_S}} \tag{10}$$

Where T_M denotes the melting point of pure iron (1809 K), and L and τ are given by Equation (11) and (12), respectively [17]:

$$L = 143.9R_c^{-0.3616}w[\mathrm{C}]^{(0.5501-1.996w[\mathrm{C}])} \tag{11}$$

$$\tau = \frac{T_L - T_s}{R_c} \tag{12}$$

Where R_c represents the cooling speed, and $w[\mathrm{C}]$ is the initial content of carbon.

The balanced distribution coefficients and diffusion rates are shown in Table 2 [9,18,19].

Table 2.
Balanced distribution coefficients and diffusion rates

Element	$k^{\gamma/L}$	D_γ, cm^2/s	D_L, cm^2/s
N	0.48	$0.91\exp\left(-\frac{250000}{RT}\right)$	$3.25\times10^{-3}\exp\left(-\frac{11500}{RT}\right)$
Ti	0.30	$0.15\exp\left(-\frac{168600}{RT}\right)$	$3.1\times10^{-3}\exp\left(-\frac{11500}{RT}\right)$

In order to illuminate the precipitation behavior of TiN inclusions in solidification, the balanced and true concentration product of TiN are represented as follows:

$$\lg(a_{\mathrm{N}} \cdot a_{\mathrm{Ti}}) = \lg K_{\mathrm{TiN}} = 5.64 - \frac{15201}{T} \tag{13}$$

$$\lg Q_{\mathrm{TiN}} = \lg(f_{\mathrm{N}} \cdot w[\mathrm{N}] \cdot f_{\mathrm{Ti}} \cdot w[\mathrm{Ti}]) \tag{14}$$

Where $\lg K_{\mathrm{TiN}}$ represents the needed equilibrium concentration product of TiN inclusions in solidification, which is governed by the solid-liquid interface temperature. When the true concentration product $\lg Q_{\mathrm{TiN}}$ exceeds the $\lg K_{\mathrm{TiN}}$, the TiN inclusions begin to precipitate and grow.

Combining the above equations with the compositions, the precipitation of TiN inclusions in liquid steel in solidification at different cooling speeds is obtained in Figure 3. This indicates that the TiN inclusions form in the mushy zone when the solid fraction is greater than 0.987. As is evident in Fig. 3, when the cooling speeds varied from 100 to 500 K/min, the influence of cooling speed on the precipitation of TiN inclusions was nearly insignificant, which is in agreement with literature [20].

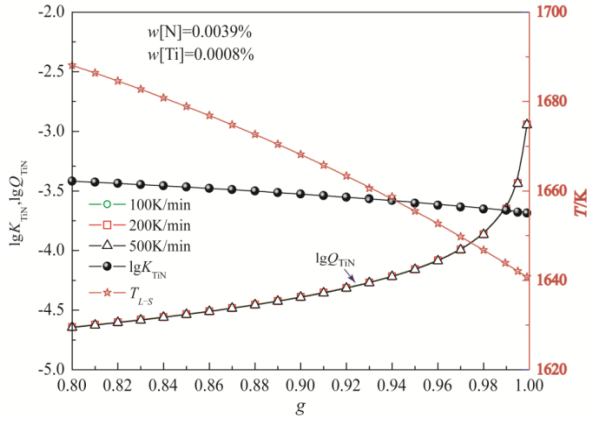

Fig. 3. Precipitation of TiN inclusions during solidification

Under actual production conditions, the thermodynamic conditions for the precipitation of TiN inclusions for different initial concentration products are shown in Figure 4. As the influence of cooling speed is nearly insignificant, the cooling speed is fixed at 500 K/min.

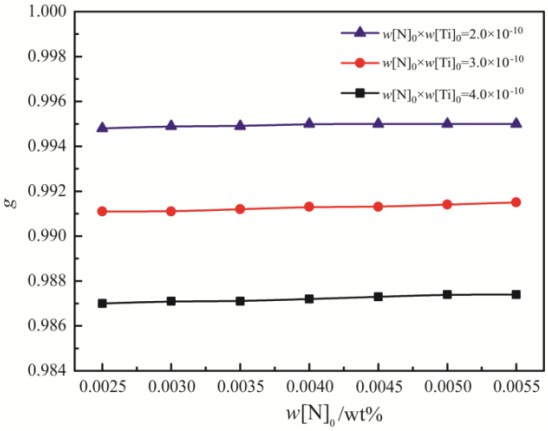

Fig. 4. Solid fraction for TiN inclusions' precipitation for various concentration products

As shown in Fig. 4, the initial concentration product obviously affects the solid fraction when TiN inclusions precipitated; the smaller the initial concentration product, the later the TiN inclusions precipitate. When the initial concentration product is the same, the solid fraction can be recorded when TiN inclusions precipitate is basically the same. Therefore, the crucial factor of TiN inclusions' precipitation is the initial concentration product.

3.3 Growth of TiN During Solidification

In liquid steel, Ti diffuses more slowly than N, so Ti is the restrictive step for the growth of TiN inclusions. The growth radius can be expressed as Equation (15) [21]:

$$r\frac{\mathrm{d}r}{\mathrm{d}t} = \frac{M_S}{100M_m}\frac{\rho_m}{\rho_s}D_L(C_L - C_e) \tag{15}$$

Where r represents the growth radius of TiN inclusions (m); t represents the growth time (s); M_m and M_S denote the molar masses of iron and TiN (g/mol), respectively; ρ_m and ρ_s represent the densities of liquid steel and TiN (g/cm^3), respectively; D_L represents the diffusion rate in liquid steel (m^2/s); and C_e is the mass concentration in equilibrium (wt%) [22].

According to above Equations, the relationship of growth size at different cooling speeds is given in Figure 5. It illustrates that the cooling speed has a significant effect on the growth radius of TiN inclusions in the solidification process. The final size of TiN inclusions decreased as the cooling speeds varied from 100 to 500 K/min; the faster the cooling speed, the smaller the final size. It also indicates that under the actual production conditions, the calculated size of the TiN inclusion is 2–5 μm, which is in reasonable agreement with the size measured in Fig. 2.

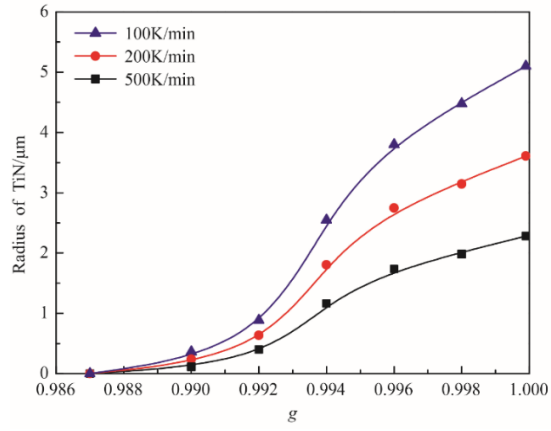

Fig. 5. Effect of cooling speed on radius of TiN inclusions

In order to make out the effect of the initial concentration product on the growth radius of TiN inclusions, the relationship between the initial concentration product and final size of TiN inclusions is given in Figure 6. It is found that when the cooling speed is fixed, the final size of TiN inclusions decreases as the N content increases for different initial concentration products. The initial concentration product has an obvious effect on the final size; the greater the initial concentration product, the larger the final radius. When the cooling speed is constant, in order to restrain the growth radius of Ti inclusions in tire cord steel, the initial concentration product can be taken into consideration. According to the production data, when the initial concentration product is controlled at a smaller value, the qualified rate of the penalty point for Ti inclusions can be improved.

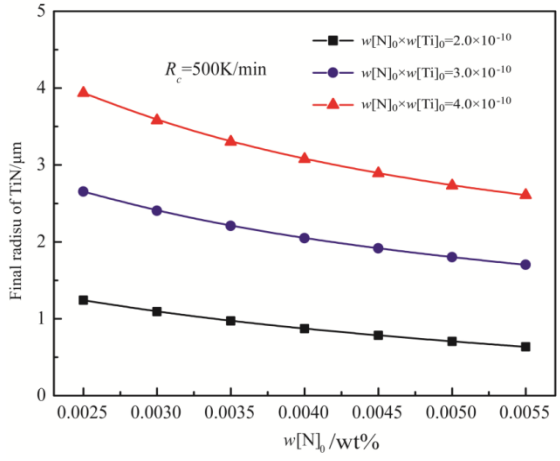

Fig. 6. Final radius of TiN at various concentration products

4. Summary

Industrial experiments show that the 2D characterization of Ti inclusions is square-like with sharp edges and corners, and the 3D shape exhibits a cubic or rectangular-prism morphology. The measuring size is in reasonable agreement with the calculations.

Mapping analysis results indicate that the Ti inclusions mainly exist in the form of TiN.

Thermodynamic calculations show that the influence of cooling speed on the precipitation of TiN inclusions is nearly insignificant. Therefore, the crucial factor of Ti inclusions' precipitation is the initial concentration product $w[N]_0 \times w[Ti]_0$.

The cooling rates significantly affect the final radius of Ti inclusions; the higher the cooling rate, the smaller the final radius. When the cooling rate is fixed, the final size is mainly determined by the initial concentration product. In order to retard the precipitation and growth of Ti inclusions, the control of cooling rate and initial concentration product are conductive.

Acknowledgments

The authors would like to thank the National Natural Science Foundation of China (Grant No. 51704105, No. 51604198).

References

[1] Parusov, V., Derevyanchenko, I., Sychkov, A., Nesterenko, A., Parusov, É. & Zhigarev, M. (2005). Ensuring high quality indices for the wire rod used to make metal cord. *Metallurgist.* 49(11-12), 439-448.

[2] Lee, S.K. , Ko, D.C. & Kim, B.M. (2009). Pass schedule of wire drawing process to prevent delamination for high strength steel cord wire. *Materials & Design.* 30(8), 2919-2927.

[3] Linaza, M.A., Romero, J.L., Rodriguezibabe, J.M., Urcola, J.J. & Ceit, S.S. (1995). Cleavage fracture of microalloyed forging steels. *Scripta Metallurgica Et Materialia.* 32(3), 395-400.

[4] Yan, W., Shan, Y.Y. & Yang, K. (2006). Effect of tin inclusions on the impact toughness of low-carbon microalloyed steels. *Metallurgical and Materials Transactions A (Physical Metallurgy and, Materials Science).* 37(7), 2147-2158.

[5] Cui, H.Z. & Chen, W.Q. (2012). Effect of boron on morphology of inclusions in tire cord steel. *Journal of Iron and Steel Research, International.* 19(4), 22-27.

[6] Li, J.Y. & Zhang, W.Y. (1989). Effect of TiN inclusion on fracture toughness in ultrahigh strength steel. *Isij International.* 29(2), 158-164.

[7] Petit, J. & Sarrazin-Baudoux, C. (2015). Fatigue crack propagation in thin wires of ultra-high strength steel. *Key Engineering Materials.* 627(1), 153-156.

[8] Liu, H.Y., Wang, H.L., Li, L., Zheng, J.Q., Li, Y.H. & Zeng, X.Y. (2011). Investigation of Ti inclusions in wire cord steel. *Ironmaking & Steelmaking.* 38(1), 53-58.

[9] Chen, J.X. (2010). *Common Charts and Databook for Steelmaking*. (2nd ed.). Beijing: Metallurgical Industry Press.

[10] Wada, H. & Pehlke, R.D. (1985). Nitrogen solubility and nitride formation in austenitic Fe-Ti alloys. *Metallurgical Transactions B (Process Metallurgy).* 16(4), 815-822.

[11] Darken, L.S. (1967). Thermodynamics of binary metallic solutions. *Trans. Metall. Soc. AIME*. 239, 80-89.

[12] Yoshikawa, T. & Morita, K. (2007). Influence of alloying elements on the thermodynamic properties of titanium in molten steel. *Metallurgical & Materials Transactions B.* 38(4), 671-680.

[13] Kim, W.Y., Jo, J.O., Chung, T.I., Kim, D. S. & Pak, J.J. (2007). Thermodynamics of titanium , nitrogen and TiN formation in liquid iron. *Isij International.* 47(8), 1082-1089.

[14] Akamatsu, S., Hasebe, M., Senuma, T., Matsumura, Y. & Kisue, O. (1994). Thermodynamic calculation of solute carbon and nitrogen in Nb and Ti added extra-low carbon steels. *Isij International.* 34(1), 9-16.

[15] Ohnaka, I. (1986). Mathematical analysis of solute redistribution during solidification with diffusion in solid phase. *Transactions of the Iron and Steel Institute of Japan,* 26(12), 1045-1051.

[16] Matsuno, J. (1976). Solidification phenomena, solidification comm. Proc. Symp. ISIJ, Tokyo.

[17] Won, Y.M. & Thomas, B.G. (2001). Simple model of microsegregation during solidification of steels. *Metallurgical and Materials Transactions A (Physical Metallurgy and, Materials Science).* 32(7), 1755-1767.

[18] Maugis, P. , & Mohamed Gouné. (2005). Kinetics of vanadium carbonitride precipitation in steel: a computer model. *Acta Materialia.* 53(12), 3359-3367.

[19] Manohar, P. A. , Dunne, D. P. , Chandra, T. , & Killmore, C. R. . (1996). Grain growth predictions in microalloyed steels. *Isij International.* 36(2), 194-200.

[20] Cai, X.F., Bao, Y.P., Wang, M., Lin, L., Dai, N. C. & Gu, C. (2015). Investigation of precipitation and growth behavior of Ti inclusions in tire cord steel. *Metallurgical Research & Technology.* 112(4), 407-417.

[21] Goto, H., Miyazawa, K., Yamada, W. & Tanaka, K. (1994). Effect of cooling speed on composition of oxides precipitated during solidification of steels. *Isij International.* 80(2), 113-118.

[22] Kunze, J., Micke, C., Backmann, G., Beyer, B., Reibold, M. & Klinkenberg, C. (1997). Precipitation of titanium nitride in low-alloyed steel during cooling and deformation. *Steel Research.* 68(10), 441-449.